ISSN 1067-8212, Russian Journal of Non-Ferrous Metals, 2025, Vol. 66, No. 3, pp. 124–136. © Pleiades Publishing, Ltd., 2025.

Diffusion Bonding of Ti_2AlNb-Based Alloy Using Spark Plasma Sintering Equipment

S. Naumov[a, *] (ORCID: 0000-0002-4084-8861), D. Panov[a, **] (ORCID: 0000-0002-8971-1268), R. Chernichenko[a] (ORCID: 0000-0002-8619-0700), V. Sokolovsky[a] (ORCID: 0000-0001-5607-2765), M. Yapryntsev[a] (ORCID: 0000-0001-8791-8102), D. Tagirov[a] (ORCID: 0009-0004-9778-4880), G. Salishchev[a] (ORCID: 0000-0002-0815-3525), and V. Lukianov[b] (ORCID: 0009-0006-3621-3966)

[a] *Laboratory of Bulk Nanostructured Materials, Belgorod State University, Belgorod, 308015 Russia*

[b] *SIA "Technopark AT", Ufa, 450027 Russia*

**e-mail: naumovstanislav@yandex.ru*

***e-mail: dimmak-panov@mail.ru*

Received May 13, 2025; revised June 25, 2025; accepted July 9, 2025

Abstract—In the present paper, the effect of diffusion bonding (DB) and post-bond heat treatment on a microstructure and mechanical properties of a Ti_2AlNb-based alloy VTI-4 was studied. DB was carried out using an SPS 10–3 selective plasma sintering system. The optimum mechanical properties of DB-joints (σ_u = 1240 MPa, $\sigma_{0.2}$ = 1070 MPa, δ = 4.6%) were achieved after DB at temperatures of 940°C and 960°C, a holding time of 120 minutes, and a pressure of 15–25 MPa. The obtained mechanical properties were equal to that of the initial material (σ_u = 1230 MPa, $\sigma_{0.2}$ = 1190 MPa and δ = 3.5%, 400 ± 10 $HV_{0.2}$). After DB at 940–960°C, microhardness was 395 ± 30 $HV_{0.2}$, which was higher than that after DB at 920°C (360 ± 25 $HV_{0.2}$). DB provoked an increase in the volume fraction of the O-phase along the joint interface compared to the base material. Post-bond heat treatment resulted in an additional increase in the volume fraction of the O-phase that increased strength and hardness.

Keywords: Ti_2AlNb-based alloy, diffusion bonding, microstructure, strength, ductility

DOI: 10.1134/S1067821225600516

INTRODUCTION

Ti_2AlNb-based alloys are attractive high-temperature materials for the aerospace industry due to their excellent properties at temperatures up to 650–700°C [1]. In particular, the alloys possess low density, high specific strength, good creep resistance, and attractive oxidation resistance [2, 3]. To obtain high-quality products using these materials, it is necessary to study their weldability [4]. During the welding processing, elastic stresses arise due to a cascade of phase transformations in different areas of the weld (fusion zone, heat-affected zone) due to low thermal conductivity and low ductility of Ti_2AlNb-based alloys, bursting the welded products [5].

For joining of Ti_2AlNb-based alloys, it is possible to use following welding techniques: tungsten arc welding (TIG), plasma welding (PW) [6], laser and electron beam welding (LBW, EBW), friction welding (FW), diffusion bonding (DB), and hybrid welding technologies [4]. However, fusion welding (TIG, PW, LBW, EBW) of Ti_2AlNb-based alloys provokes the formation of a weld seam with a coarse-grained B2-phase that decreases mechanical properties of the welded joint dramatically. Due to preserving the coarse-grained microstructure of the fusion zone, post-weld heat treatment somewhat increases strength and ductility of the welded joints [7, 8].

On the other hand, DB of Ti_2AlNb-based alloys provide a good combination of mechanical properties of obtained uniform or dissimilar joints [9]. To prevent the formation of brittle intermetallics during dissimilar bounding [10] or limit the joining line and coagulation of the O-phase at the diffusion joint interface [11], it is suggested to use an intermediate layer, namely foils made of pure Ti [12] or high-entropy alloys (TiZrHfNbAl, AlNbHfTaTi, etc.). However, tuning of DB parameters can also inhibit the coagulation of the O-phase during the processing.

To attain a high-quality joint, spark plasma sintering (SPS) equipment is also used. The processing is implemented using pulsed current and applied pressure [13, 14], which can essentially be called resistance butt welding. The use of SPS equipment is possible and relevant for DB, but it is required that the pulse

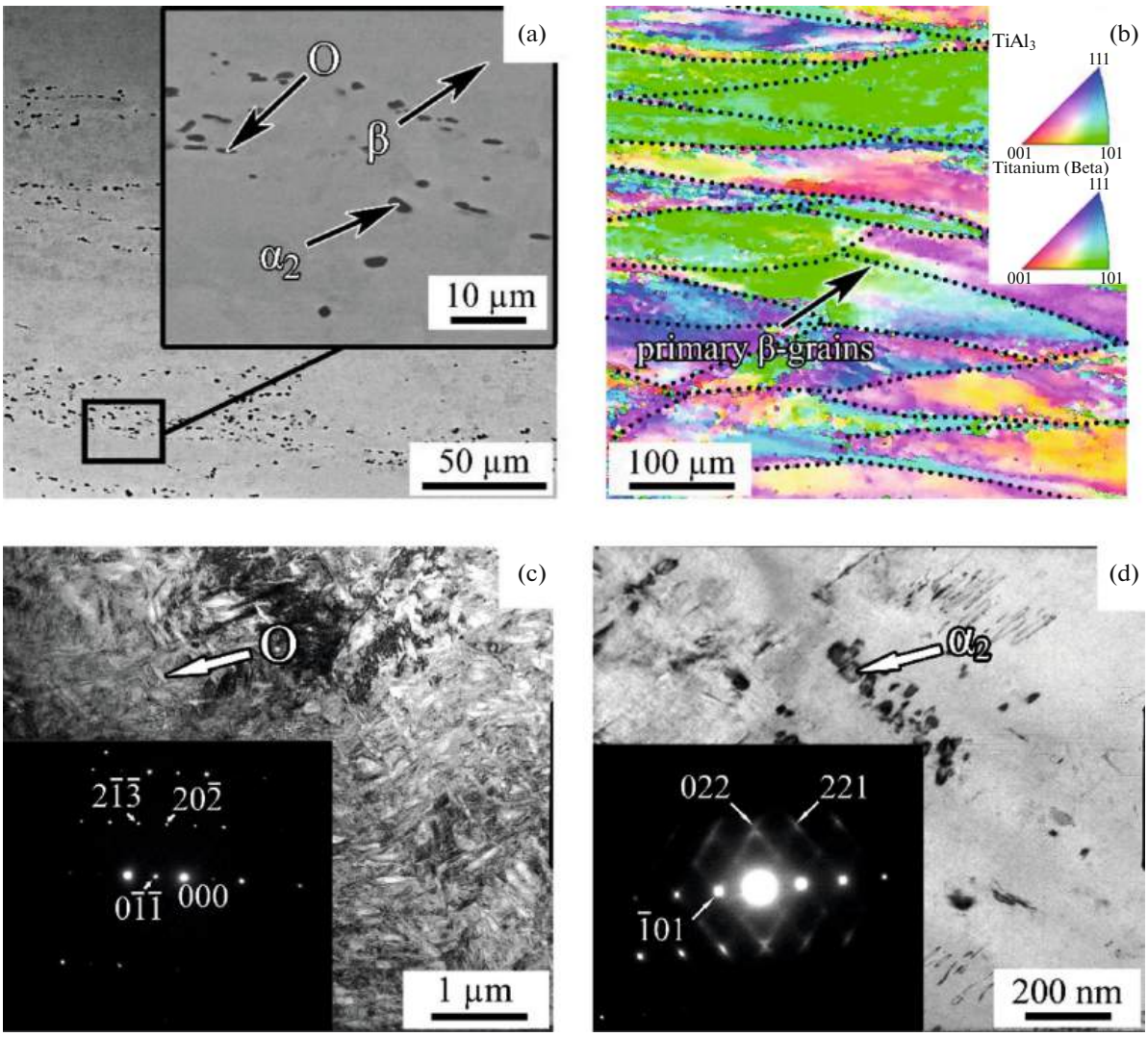

Fig. 1. Initial microstructure of the alloy VTI-4: (a) BSE analysis; (b) EBSD analysis; (c–d) TEM image.

current passes through the graphite matrix and punches but not through the bonded blanks. The approach can be combined with hot deformation of Ti_2AlNb/TiAl-based alloys, which improves the mechanical properties of DB-joints [15].

Post-bond heat treatment (PBHT) is a pathway for further strengthening, adjusting the microstructure of DB-joints. In particular, after DB, aging at 600°C (O-phase area) [16] or at 850°C (O + β phase area) [17] is applied. Since the β-phase is metastable and transforms at high temperatures ($\beta \rightarrow O$ and/or $\beta \rightarrow \alpha_2$), PBHT can stabilize the structure and properties of the obtained joints [4]. However, the most common PBHT mode is solution treatment at temperatures of the β-phase region and aging at 800–840°C to precipitate the O-phase [7].

Thus, the aim of this work is to study the effect of DB modes using SPS equipment and PBHT on a microstructure and mechanical properties of a Ti_2AlNb-based alloy.

EXPERIMENTAL

Program Material

The hot-forged plate of a Ti_2AlNb-based alloy VTI-4 was studied. The program alloy possessed the chemical composition: Ti–23Al–23Nb–1.4V–0.8Zr–0.4Mo–0.4Si (at %). In the initial state, the alloy VTI-4 performed the following mechanical properties: σ_u = 1230 MPa, $\sigma_{0.2}$ = 1190 MPa, and δ = 3.5%. Microhardness of the initial plate was 400 ± 10 $HV_{0.2}$. The microstructure of the initial plate consisted of a β-matrix, a lamellar O-phase and a globular α_2-phase (Fig. 1). The program alloy had the subsequent phase composition: 15% of O-phase, 21% of α_2-phase, and 64% of β-phase. In β, α_2 and O phases

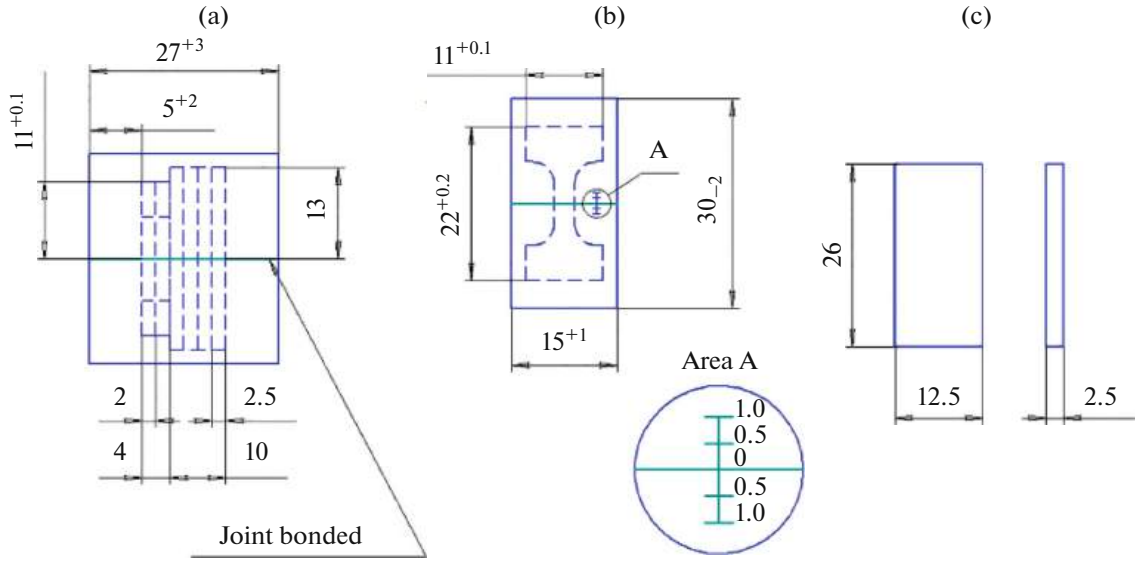

Fig. 2. Scheme of cutting samples from DB-joints: (a) for mechanical testing; (b) scheme of cutting a sample for uniaxial tension and a section for measuring microhardness (area A); (c) for PBHT.

the content of Nb and Al was different. The darkest particles in BSE images were the α_2-phase (Ti_3Al), whereas the lighter particles were the O-phase (Ti_2AlNb). The light background was the β-matrix (Ti) [18]. The size of the elongated β-grains was 460 ± 110 μm in length and 105 ± 40 μm in thickness (Fig. 1b). Along boundaries of β-grains, a diameter of globular α_2-particles was less than 1.5 μm. Particles of the lamellar O-phase with a length of 0.1–3.5 μm and a thickness of 0.1–1.5 μm were uniformly distributed (Fig. 1c).

Diffusion Bonding and Post-bond Heat Treatment

The main design and technological requirements for DB of Ti_2AlNb-based alloys were summarized below:

— Before DB, the mating surface of the samples should be ground with sandpaper followed by mechanical polishing to reduce surface roughness [19]. Samples must be ultrasonically cleaned in an acetone bath (C_2H_5OH, carbon 4-chloride or other solvents) for 15–30 min. The surface after mechanical and physical-chemical treatment must be brought to 4–6 class of cleanliness (GOST 2789–59).

— The vacuum during DB of Ti_2AlNb-based alloy should be 1×10^{-2} Pa or higher [20, 21]. However, according [22], the DB-joint TiAl–Nb–TiAl was also obtained in a vacuum of 4.5×10^{-1} Pa.

— The elastic strength of the Ti_2AlNb-based alloy was ≈20 MPa, which limits the applied pressure during DB. Therefore, the pressure should be selected within a loading range of 8–20 MPa [13, 23].

— Depending on the Nb concentration, upper boundary of the β/B2 + O phase region was located at a temperature of 960 or 980°C. Therefore, the temperature range of DB was from 900 to 980°C [24–27].

— The holding time of samples during DB varied from 10 to 210 min depending on the temperature and applied pressure [23, 24].

— Cooling of DB-joints was carried out together with the furnace (chamber) of the DB equipment [19].

Based on the listed requirements for DB, a spark plasma sintering system SPS 10–3 was selected. The system is comparable for obtaining a high-quality DB-joint of Ti_2AlNb-based alloys. Samples for DB measuring $27 \times 15 \times 15$ mm^3 were cut from the hot-forged plate (Fig. 2a). Before DB, the mating surfaces were ground with sandpaper, followed by mechanical polishing and ultrasonic cleaning in an acetone bath for 15–30 min.

Parameters of DB are presented in Table 1. Vacuum in the chamber was 2×10^{-2} Torr. Three times purging with argon grade 6.0 was used. Thus, the heating of the samples was carried out by radiation from a graphite matrix with an internal diameter of 40 mm. To reduce heat loss due to heating, the graphite matrix was thermally insulated with fiber. A pulsed current for heating passed through two graphite punches (*1*, *6*) and a graphite matrix (*3*). The samples (*4*) were placed in the central part of the matrix and isolated from electric current by corundum inserts (*2*). In order to precisely place and load the samples without shifting them, titanium foil made of VT1-00 (*5*) was used before DB, and the area between the samples and the matrix was filled with titanium shavings. When the

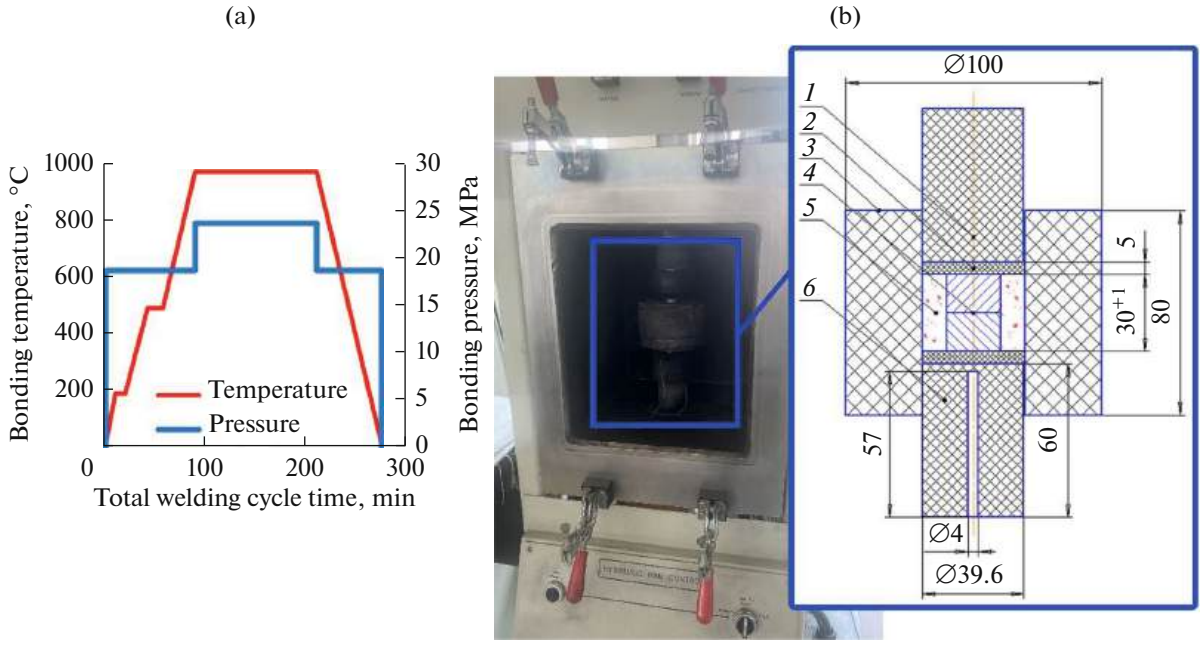

Fig. 3. (a) welding cyclogram of VTI-4 alloy on SPS 10-3 equipment; (b) device for placing samples inside the chamber: (*1*) upper punch; (*2*) corundum insert; (*3*) graphite matrix; (*4*) welded samples; (*5*) titanium shavings; (*6*) lower punch.

temperature reached 200°C during heating, a pause was maintained to remove combustion products from the chamber (Fig. 3a). The second pause was carried out at 500°C to reduce the temperature gradient and final degassing of combustion products in the chamber [28]. The bonding cycle was divided into three stages, namely heating, holding and cooling with continuous temperature recording. The thermocouple was located in the lower graphite punch at a distance of 3 mm from the mating surface with the sample (Fig. 3b). Cooling of the welded samples was carried out together with the furnace (chamber).

PBHT of DB-joints was conducted in a furnace Nabertherm LT 5/12/P320 with following modes: PBHT1—heating to 920°C (α_2 + β + O-phase region), holding for 2 h and air cooling, followed by aging for 6 hours at a temperature of 800°C (β + O-phase region) with air cooling; PBHT2—heating to 960°C (α_2 + β + O-phase region), holding for 2 hours and air cooling, followed by aging for 6 h at a temperature of 800°C (β + O-phase region) with air cooling.

Mechanical Testing and Microstructure Characterization

Uniaxial tensile tests were performed using a universal testing machine Instron 5882 at room temperature with a strain rate of 10^{-4} s^{-1}. The scheme of the sample is shown in Fig. 2b. Control and data collection were carried out using the Instron Bluehill 2 software. The microhardness value was estimated on samples in the cross-section of DB-joints according to

Table 1. Modes of diffusion bonding

No.	Temperature, °C	Holding time, min	Pressure, MPa	Heating rate, °C/min	Cooling rate, °C/min
1	920	120	15	15	15
2	940	120	15	15	15
3	960	120	15	15	15
4	980	120	15	15	15
5	960	120	25	15	15

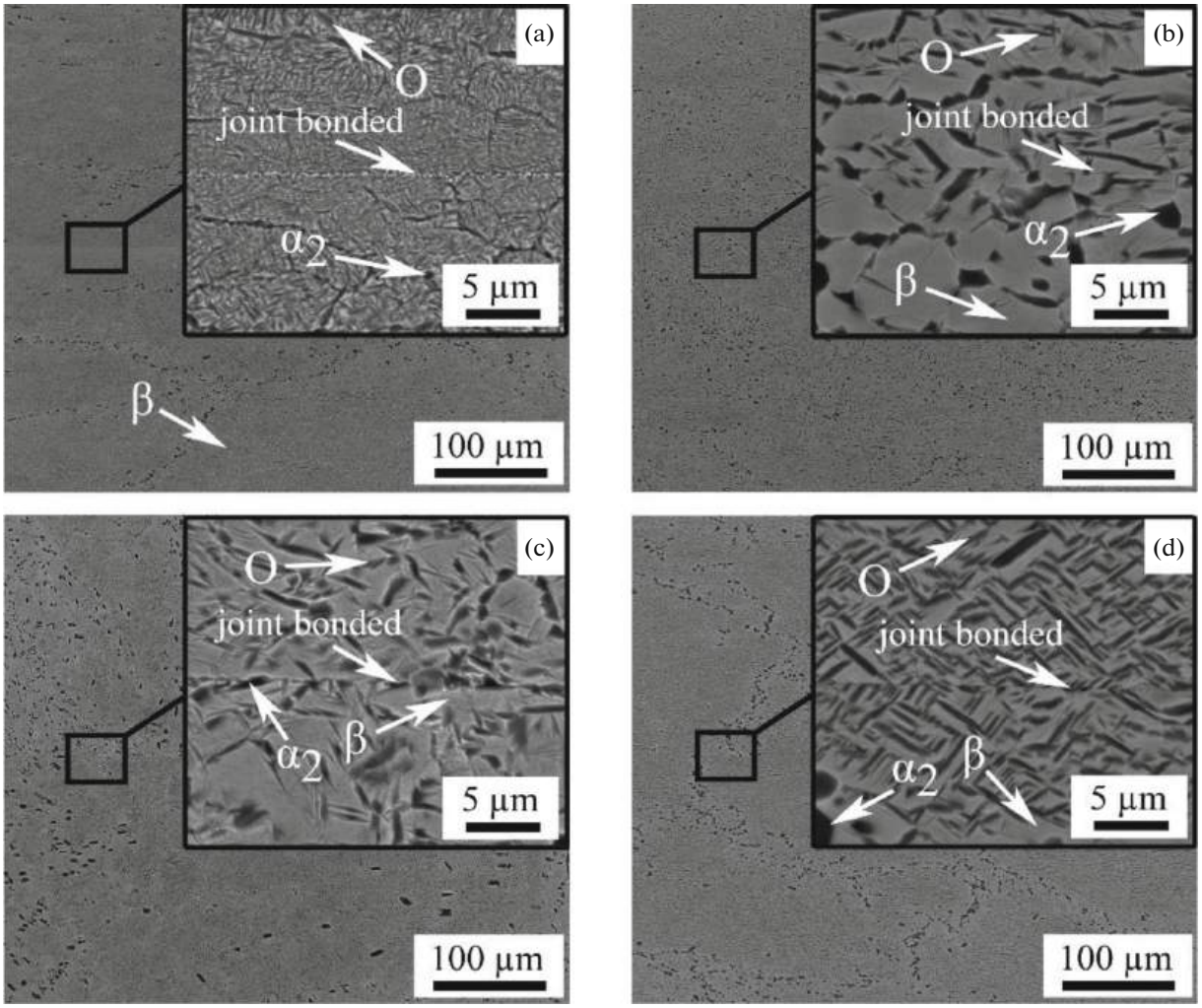

Fig. 4. BSE analysis of DB-joints obtained at: (a) 920°C, 15 MPa; (b) 940°C, 15 MPa; (c) 960°C, 15 MPa; (d) 980°C, 15 MPa.

ISO 22826 (Fig. 2b, area A). The measurements were conducted with a step of 80 μm using a Vickers microhardness tester Wolpert 402MVD with a load of 0.2 kg and an indentation time of 15 s ($HV_{0.2}$).

The microstructure was studied using a FEI Quanta 200 3D scanning electron microscope at 30 kV. EBSD-analysis was performed using a Nova NanoSEM 450 microscope equipped with an EDAX Hikari EBSD camera at 30 kV. The initial microstructure was also studied using a JEOL JEM-2100 transmission electron microscope at 200 kV. The 300 μm thick foil blanks were cut using electrical discharge cutting and then thinned to 100 μm on a LaboPol-5 mechanical grinding and polishing machine. These samples were then subjected to dual-jet electrolytic polishing and perforation using Tenupol-5 with an electrolyte consisting of 60 mL $HClO_4$, 600 mL CH_3OH and 360 mL C_4H_9OH, at 27 V and −30°C. After perforation, the foils were cleaned in distilled water and ethyl alcohol.

RESULTS AND DISCUSSION

Microstructure Characterization of DB-joints

The microstructure of the DB-joints consisted of a β-matrix, a lamellar O-phase, and a small amount of equiaxed α_2-phase (Fig. 4). As Shown in Fig. 4a, after DB at 920°C, the average length of the O-phase in the base metal was 2.71 ± 0.2 μm, while the average length of the O-phase at the DB-joint boundary was 0.87 ± 0.2 μm. After DB at 940°C, the average length of the O-phase in the base metal was 2.27 ± 0.2 μm, and those located at the boundary of the DB-joint was 1.62 ± 0.1 μm (Fig. 4b). After DB at 960°C, the average length of the O-phase in the base metal and at the boundary of the DB-joint decreased to 1.7 ± 0.2 μm and to 1.37 ± 0.1 μm, respectively (Fig. 4c). After DB at 980°C (Fig. 4d), the average length of the O-phase in the base metal and at the boundary with the DB-joint reached 2.98 and 1.91 μm, respectively.

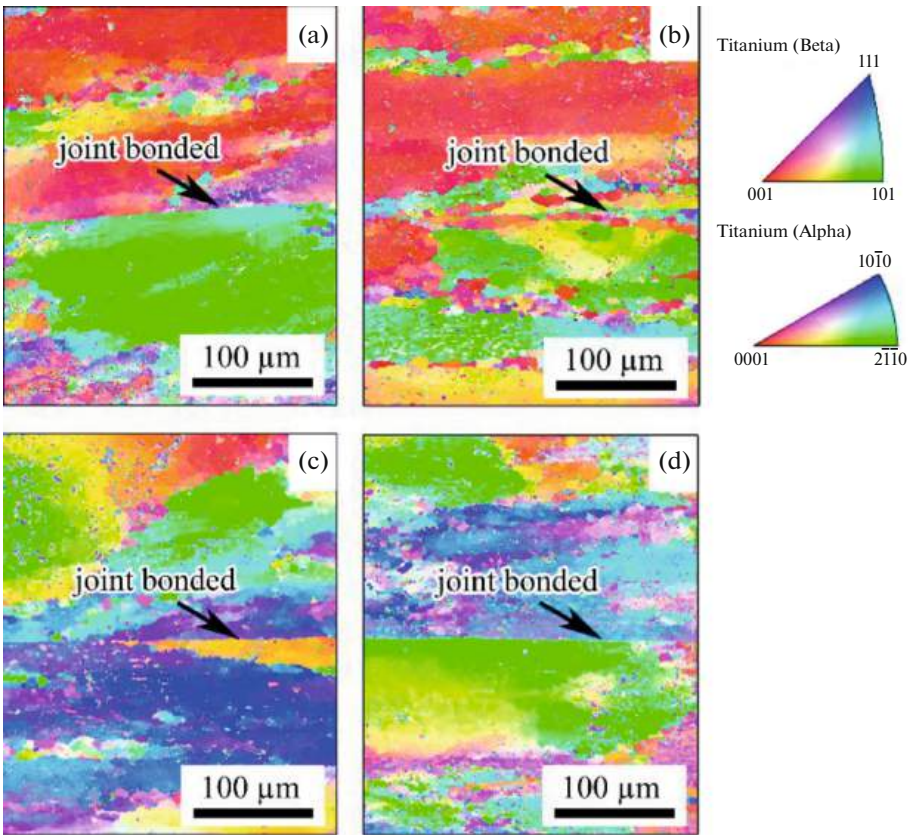

Fig. 5. EBSD analysis of DB-joints: (a) 920°C, 15 MPa; (b) 940°C, 15 MPa; (c) 960°C, 15 MPa; (d) 980°C, 15 MPa.

Figure 5 presents EBSD-maps of DB-joints obtained at different temperatures. Along the boundaries of large β-grains, smaller grains (≈20 μm) were observed, where an increased fraction of the α_2-phase was detected. Only β- and O-phases were attained at the site of the DB line of large primary β-grains (Fig. 4). No distinctive microstructural features were found in the of diffusion joints obtained at different welding temperatures.

Mechanical Testing of DB-joints

Microhardness of DB-joints was in a range of 336–425 $HV_{0.2}$ (Fig. 6). The minimum microhardness value of 360 ± 25 $HV_{0.2}$ was obtained after DB at 920°C (Fig. 6a) due to the increased content of the α_2-phase and the higher content of the O-phase. Yet, the maximum value of microhardness 395 ± 30 $HV_{0.2}$ was achieved after DB at 940 and 960°C.

According to the results of tensile testing (Fig. 6b), the strength of DB-joints increased with increasing the processing temperature. Thus, at a DB temperature of 940–960°C, the ultimate strength (σ_u) and yield strength ($\sigma_{0.2}$) were 1180 and 1010 MPa, respectively. These values of the strength of DB-joints were more than 95% of the base-metal strength. At 980°C, the strength increased to the same strength as the initial metal, which was associated with an increase in the volume fraction of the O-phase. However, soon fracture occurred along the DB-joint, and the ductility did not exceed 1%.

Increasing the pressure from 15 to 25 MPa during DB at 960°C improved the mechanical properties of the DB-joint. This ensured the equal strength of the DB-joint relative to the initial metal, while ductility increased by 1.5 times. The samples were damaged along the base metal or the crack partially propagates in the base metal and diffusion bonding joint (Fig. 6c). The microhardness level of DB-joints did not change with increasing pressure (15 MPa—395 ± 30 $HV_{0.2}$; 25 MPa—385 ± 25 $HV_{0.2}$). However, the shrinkage of ≈10% was observed after the processing.

Figure 7 shows the fracture surfaces of DB-joints after tensile tests. As can be seen in Fig. 7a after DB at 920°C and 15 MPa, the fracture surface was a connection plane between the samples, which made it flat and smooth. On the fracture surface of samples obtained at DB temperatures of 940 and 960°C

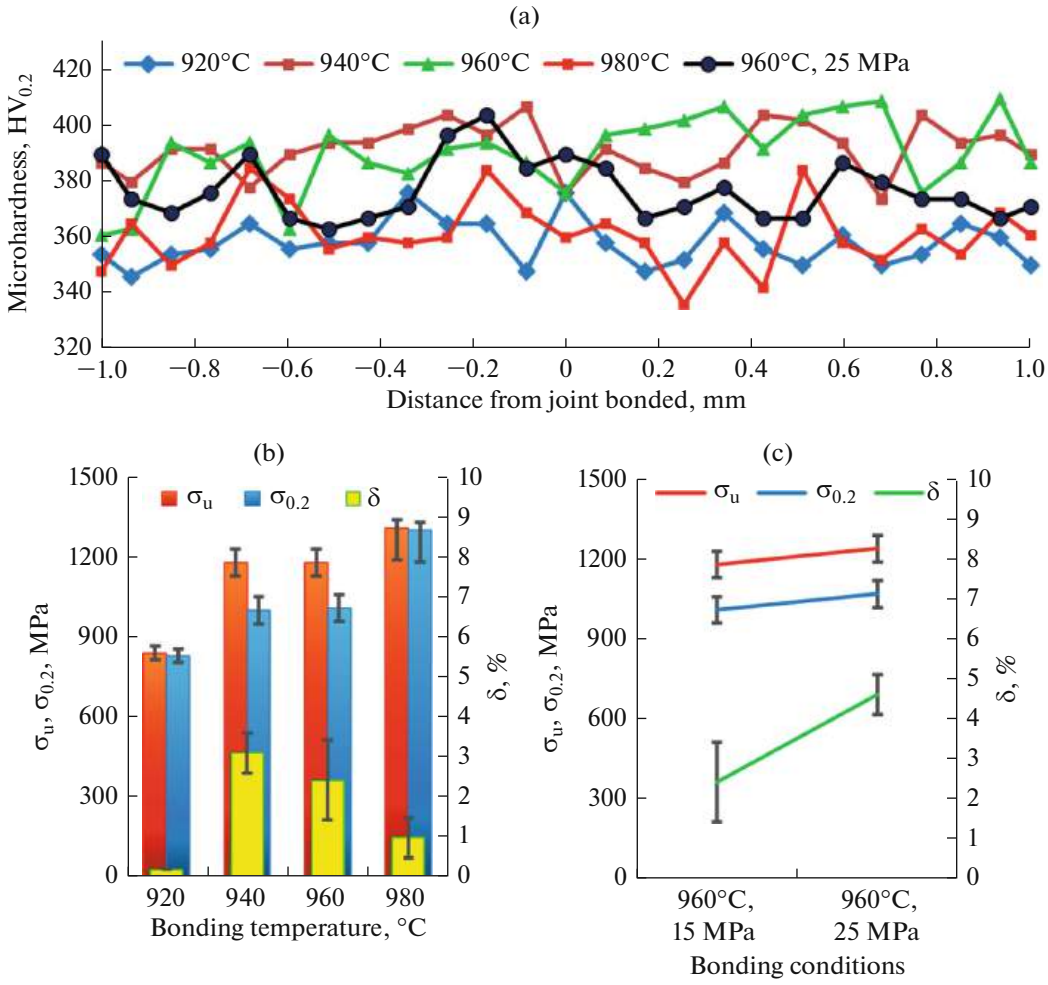

Fig. 6. (a) Microhardness of DB-joints depending on welding modes; (b) mechanical properties of DB-joints; (c) mechanical properties of DB-joints at 960°C depending on the welding pressure.

(Figs. 7b–7c), facets of quasi-cleavage and transgranular fracture as well intergranular cracking were observed. This demonstrated the good quality of the DB-joints, which possessed higher plastic properties. After DB at 980°C, fewer deformation zones were found on the fracture surface (Fig. 7d) that indicated lower ductility.

Effect of PBHT on the Microstructure and Mechanical Properties of DB-joints

Figures 8 and 9 show microstructures of the obtained DB-joints after PBHT1 and PBHT2 depending on the DB conditions. PBHT of DB-joints after DB at a pressure of 25 MPa was not considered, since, at such a condition, the sample were deformed more than 10%.

The microstructure of DB-joints consisted of a β-matrix, a lamellar O-phase and a small amount of equiaxed α_2-phase particles. However, after PBHT, the volume fraction of O- and α_2-phases varied depending on the DB temperature. With increasing DB temperature, the amount of O-phase increased (Table 2), while the amount of α_2-phase was stable. Apparently, after PBHT2, the volume fraction of α_2-phase increased by ~2 times compared to PBHT1.

Microhardness of the DB-joint after PBHT1 was 350 ± 20 $HV_{0.2}$, whereas microhardness of the DB-joint after PBHT2 was 400 ± 30 $HV_{0.2}$. In both cases, with increasing DB temperature, the microhardness increased slightly. Microhardness peaks were also found in the joint area at point "0" at 920 and 980°C after PBHT1 (Fig. 10a) and 960°C after PBHT2 (Fig. 10b).

After PBHT1, σ_B and $\sigma_{0.2}$ of the joint bonded at 960°C were 1020 MPa and 930 MPa, respectively, which is more than 80% of the base metal strength. Moreover, ductility increased by more than 1.5 times and reached 6.2% (Figs. 11a, 11b). For the joint

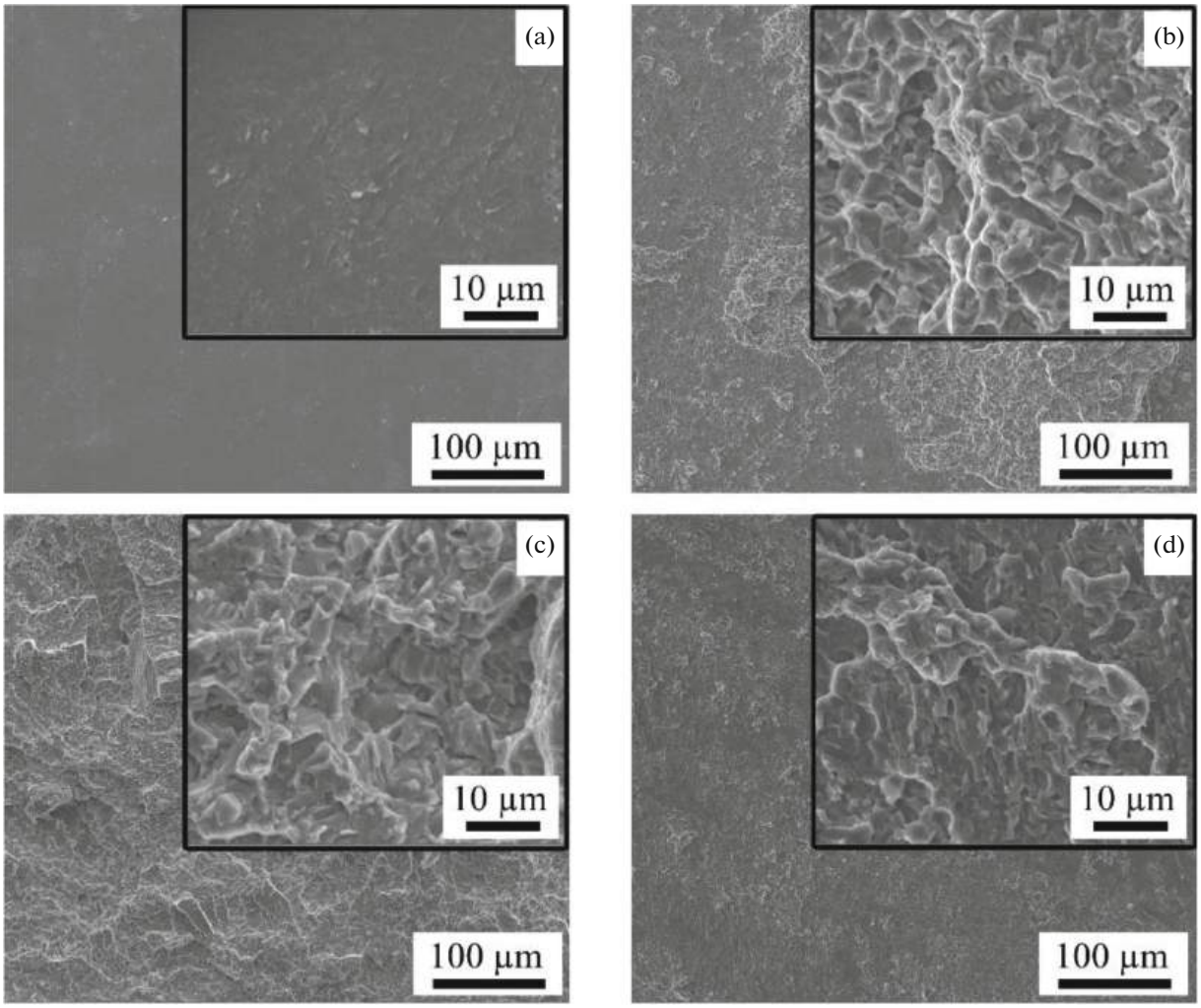

Fig. 7. Fractography of DB-joints obtained at: (a) 920°C, 15 MPa; (b) 940°C, 15 MPa; (c) 960°C, 15 MPa; (d) 980°C, 15 MPa.

bonded at 940°C, the ductility was slightly lower than that at 920 and 960°C.

After PBHT2, σ_u and $\sigma_{0.2}$ of joints bonded at 960°C were 1210 and 1160 MPa, respectively, that was equal to the initial metal strength. However, the ductility remained at the same low level (Figs. 11a, 11c). The mechanical properties of joints bonded at 940 and 960°C after PBHT2 differed from PBHT1. So, strength increased by up to ~20% and ductility decreased by ~2 times due to an increase in the content of the α_2 phase.

Thus, heat treatment allows regulating the strength and plastic properties of DB-joints in a wider range. A comparative analysis of weldability (by weld strength

Table 2. Phase composition of the DB-joints after PBHT1

Welding mode, °C		920	940	960	980
Average value, %	O-phase	50.49	60.81	72.67	76.72
	α_2-phase	2.40	7.05	11.26	6.75

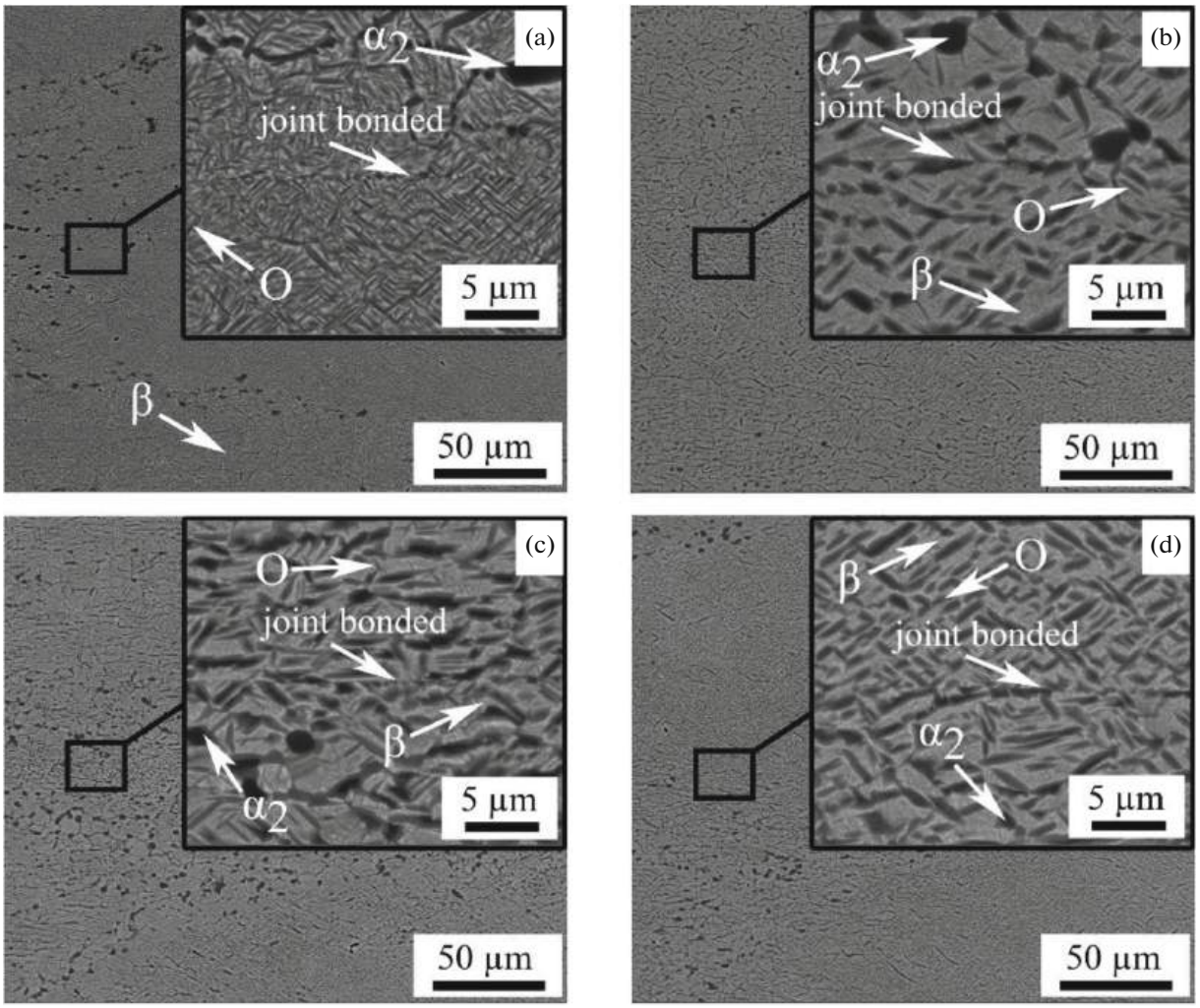

Fig. 8. BSE analysis of the diffusion bonding joints of VTI-4 alloy obtained after PBHT1: (a) 920°C, 15 MPa; (b) 940°C, 15 MPa; (c) 960°C, 15 MPa; (d) 980°C, 15 MPa.

and ductility) of VTI-4 alloy was conducted (Fig. 12). The mechanical properties of welded joints obtained by fusion (blue area) [6, 29, 30] and DB (green area) were different. Apparently, DB provided the better strength-ductility combination of DB-joints due to the absence of a fusion zone and HAZ, and as a consequence a finer microstructure.

CONCLUSIONS

In the current work, the effect of diffusion bonding (DB) modes using SPS 10-3 equipment and PBHT on the microstructure and mechanical properties of Ti_2AlNb-based alloys is studied. Following conclusions are drawn:

(1) The best mechanical properties of DB-joints of the Ti_2AlNb-based alloy VTI-4 are achieved after DB at temperatures of 940 and 960°C, a holding time of 120 min, a pressure of 15 ± 1 MPa (σ_u = 1180 MPa, $\sigma_{0.2}$ = 1010 MPa, ≈95% of the initial metal strength, δ = 3%) and at a temperature of 960°C, a pressure of 25 ± 1 MPa (σ_u = 1240 MPa, $\sigma_{0.2}$ = 1070 MPa, δ = 4.6%, which ensures equal to the initial metal strength).

(2) After DB at 940–960°C, the microhardness is 395 ± 30 $HV_{0.2}$, which is higher than at 920°C (360 ± 25 $HV_{0.2}$), and is close to the initial material microhardness (400 ± 10 $HV_{0.2}$). Meanwhile, ductility of DB-joints increases with increasing DB temperature from 920 to 960°C at a pressure of 15 ± 1 MPa and reaches 3.8%. With an increase in DB temperature,

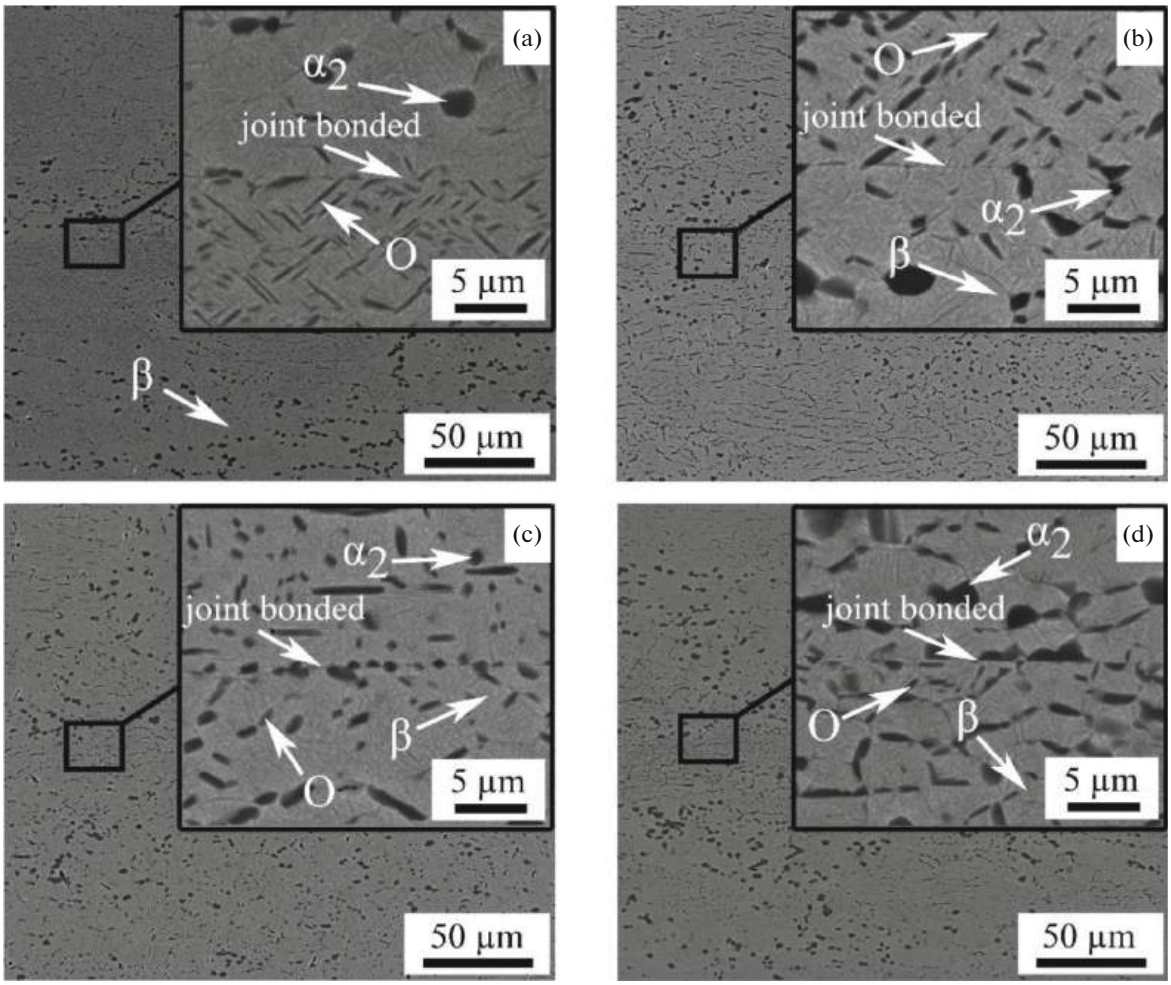

Fig. 9. BSE analysis of PBHT2 joints obtained DB at: (a) 920°C, 15 MPa; (b) 940°C, 15 MPa; (c) 960°C, 15 MPa; (d) 980°C, 15 MPa.

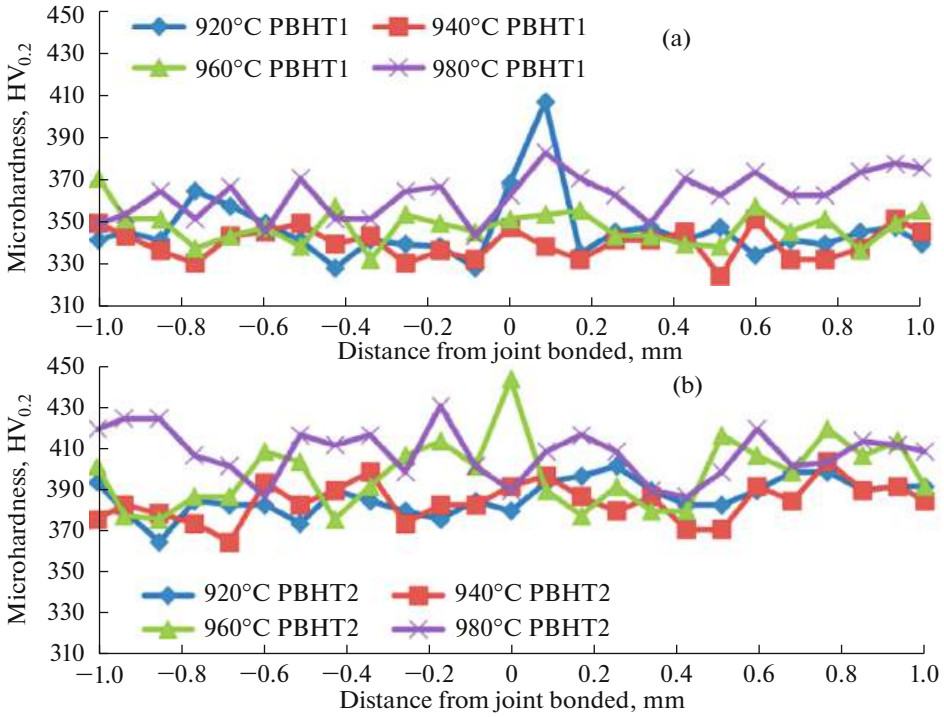

Fig. 10. Microhardness of DB-joints after: (a) PBHT1; (b) PBHT2.

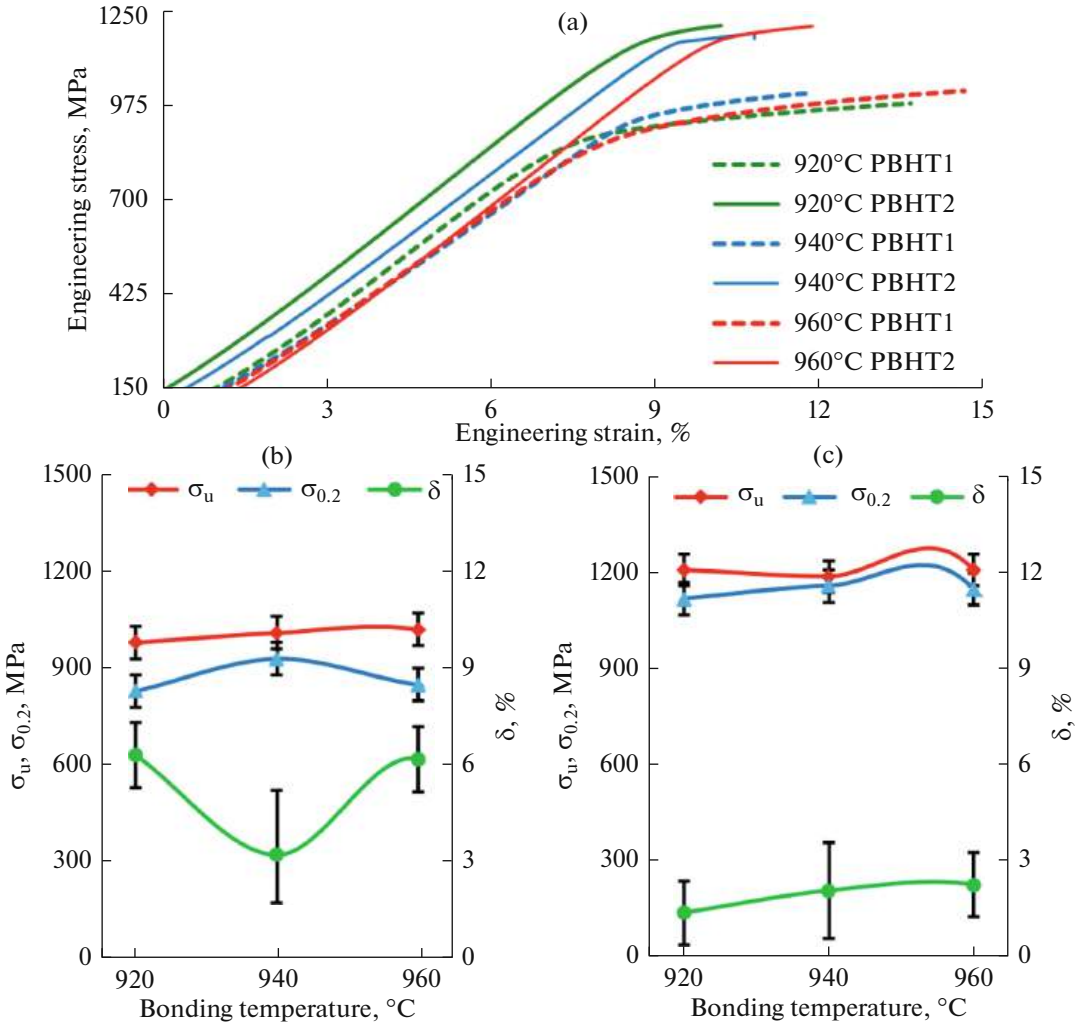

Fig. 11. Mechanical properties of DB-joints after PBHT depending on welding temperature: (a) tension diagrams, (b) mechanical properties after PBHT1; (c) mechanical properties after PBHT2.

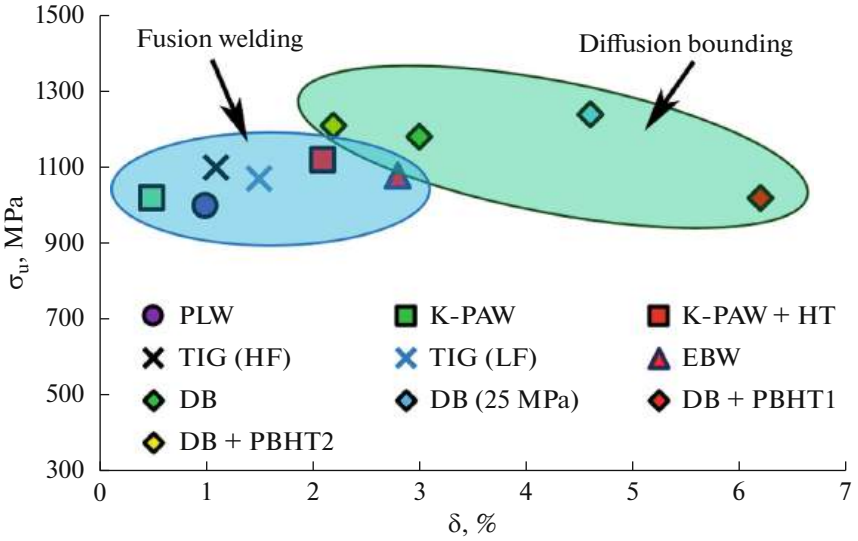

Fig. 12. Ultimate strength (σ_u) and ductility (δ) combination of the joints of the alloy VTI-4 obtained using different welding techniques: K-PAW—keyhole plasma arc welding, HT—subsequent heat treatment [6], PLW—pulse laser welding [29], TIG (LF)—tungsten inert gas welding with low-frequency pulses, TIG (HF)—using direct current with high-frequency pulses [30], EBW—electron beam welding, DB—diffusion bonding, PBHT—post-bond heat treatment. Blue area—fusion welding, green area—diffusion bounding.

the fraction of the O-phase and α_2-phase in the DB-joints increases (940°C: 44.58% O-phase, 6.45% α_2-phase; 960°C: 54.05% O-phase, 9.9% α_2-phase).

(3) After PBHT of DB-joints, the fraction of O- and α_2-phase increases with an increase in DB temperature (940°C—60.81% O-phase, 7.05% α_2-phase; 960°C—72.67% O-phase, 11.26% α_2-phase). Increasing the fraction of the O-phase and α_2-phase in the DB-zone leads to the rise of strength and hardness. The PBHT1 mode (heating at 920°C, holding for 2 h and air cooling, followed by aging for 6 hours at a temperature of 800°C with air cooling) improves ductility to $\delta = 6\%$ with some reduction in strength characteristics. The PBHT2 mode (heating at 960°C, holding for 2 h and air cooling, followed by aging for 6 h at a temperature of 800°C with air cooling.) provides strength and ductility equal to those of the initial material. Depending on the requirements for the properties of a specific DB-joint, subsequent heat treatment allows for flexible control of its mechanical characteristics.

ABBREVIATIONS AND NOTATION

DB	diffusion bonding
BSE	backscattered electrons
EBSD	electron backscatter diffraction
PBHT	post-bond heat treatment
SPS	spark plasma sintering

FUNDING

This work was supported by the Russian Science Foundation (grant no. 19-79-30066) using the equipment of BSU Shared Research Facilities “Technologies and Materials”.

CONFLICT OF INTEREST

The authors of this work declare that they have no conflicts of interest.

REFERENCES

1. Kumpfert, J., Intermetallic alloys based on orthorhombic titanium aluminide, *Adv. Eng. Mater.,* 2001, vol. 3, pp. 851–864. https://doi.org/10.1002/1527-2648(200111)3:11<851::AIDADEM851>3.0.CO;2-G
2. Liu, S.S., Cao, J.X., Zhou, Y., Dai, S.L., Huang, X., and Cao, C.X., Research and prospect of Ti_2AlNb alloy, Zhongguo Youse Jinshu Xuebao/*Chin. J. Nonferrous Met.,* 2021, vol. 31, pp. 3106–3126. https://doi.org/10.11817/j.ysxb.1004.0609.2021-42420
3. Illarionov, A.G., Demakov, S.L., Vodolazskiy, F.V., Stepanov, S.I., Illarionova, S.M., Shabanov, M.A., and Popov, A.A., Alloys Based on Orthorhombic Intermetallic Ti_2AlNb: Phase Composition, Alloying, Structure, Properties, *Metallurgist,* 2023, vol. 67, pp. 305–323. https://doi.org/10.1007/s11015-023-01518-z
4. Zou, J. and Li, H., Review on weldability of Ti_2AlNb-based alloy, *Mater. China,* 2019, vol. 38, pp. 710–716. https://doi.org/10.7502/j.issn.1674-3962.201803012
5. Li, Y., Wu, A., Li, Q., Zhao, Y., Zhu, R., and Wang, G., Mechanism of reheat cracking in electron beam welded Ti_2AlNb alloys, *Trans. Nonferrous Met. Soc. China,* 2019, vol. 29, pp. 1873–1881. https://doi.org/10.1016/S1003-6326(19)65095-8
6. Naumov, S.V., Panov, D.O., Chernichenko, R.S., Sokolovsky, V.S., Salishchev, G.A., Alekseev, E.B., Neulybin, S.D., Belinin, D.S., Shchitsyn, Y.D., and Lukianov, V.V., Structure and mechanical properties of Ti_2AlNb-based alloy welded joints using keyhole plasma arc welding with subsequent heat treatment, *Izv. Non-Ferrous Metall.,* 2024, vol. 30, pp. 16–29. https://doi.org/10.17073/0021-3438-2024-2-16-29
7. Wu, Y., Liu, G., Liu, Z.-Q., Tang, Z.-J., and Wang, B., Microstructure, mechanical properties and post-weld heat treatments of dissimilar laser-welded Ti_2AlNb/Ti60 sheet, *Rare Met.,* 2023, vol. 42, pp. 1332–1342. https://doi.org/10.1007/s12598-018-1047-5
8. Panov, D., Naumov, S., Stepanov, N., Sokolovsky, V., Volokitina, E., Kashaev, N., Ventzke, V., Dinse, R., Riekehr, S., Povolyaeva, E., et al., Effect of pre-heating and post-weld heat treatment on structure and mechanical properties of laser beam-welded Ti_2AlNb-based joints, *Intermetallics,* 2022, vol. 143, p. 07466. https://doi.org/10.1016/j.intermet.2022.107466
9. Chen, Y., Cheng, Y., Zhao, C., Zhan, L., Zhou, T., and Wang, G., Analysis of the interfacial microstructure, phase transformation, and diffusion mechanism of Ti_2AlNb/TA2 joint diffusion-bonded at low temperature, *Mater. Charact.,* 2024, vol. 209, p. 113732. https://doi.org/10.1016/j.matchar.2024.113732
10. Li, P., Wang, Y., Zhang, L., Li, C., Zhang, Z., and Dong, H., High strength diffusion bonding of Ti_2AlNb to GH4169 with (TiZrHfNb)95Al5 high entropy interlayer, *Mater. Sci. Eng., A,* 2024, vol. 902, p. 146558. https://doi.org/10.1016/j.msea.2024.146558
11. Du, S., Hu, H., and Ding, K., Microstructure of γ-TiAl and Ti_2AlNb linear friction welding joint, *Acta Aeronaut. Astronaut. Sin.,* 2024, vol. 45, p. 629347. https://doi.org/10.7527/S1000-6893.2023.29347
12. Chen, H., Bu, Z., Zhou, Y., Huang, X., and Li, J., Microstructure and mechanical properties of Ti_2AlNb joints diffusion bonded using Ti foils as interlayer, *Intermetallics,* 2025, vol. 181, p. 108731. https://doi.org/10.1016/j.intermet.2025.108731
13. Ma, M., Chen, C., Chai, L., Lv, Y., Hou, J., and Zhang, B., Effect of welding temperature on microstructure and mechanical properties of TiAl/Ti_2AlNb spark plasma diffusion welded joint, *Weld. World,* 2022, vol. 66, pp. 985–994. https://doi.org/10.1007/s40194-021-01247-4
14. Zhang, B., Chen, C., He, J., Hou, J., Chai, L., and Lv, Y., Spark plasma diffusion bonding of TiAl/Ti2AlNb with Ti as interlayer, *Materials* (Basel), 2020, vol. 13, pp. 1–9. https://doi.org/10.3390/ma13153300

15. Zhu, L., Wang, X., Chen, Y., Wei, B., Zheng, G., Fan, Z., Zou, J., Tang, B., and Li, J., Enhanced tensile strength of TiAl/Ti2AlNb diffusion bonding joint by a novel post-bonded hot deformation, *J. Mater. Res. Technol.,* 2024, vol. 29, pp. 3598–3605. https://doi.org/10.1016/j.jmrt.2024.02.115

16. Du, Y.J., Xiong, J.T., Jin, F., Li, S.W., Li, J.L., Gao, X.Y., Wang, Z.N., Wen, G.D., and Guo, W., Nanophase strengthening Ti_2AlNb diffusion bonding joint using refractory high entropy interlayer and post-bond heat treatment, *Mater. Charact.,* 2023, vol. 196, p. 112593. https://doi.org/10.1016/j.matchar.2022.112593

17. Zhou, M., Li, J., Zhang, K., Xiong, J., Li, J., and Du, Y., Precipitation behavior and strengthening mechanism of the interfacial nano-O phase of Ti_2AlNb diffusion welded joints with high-entropy interlayer during aging process, *Mater. Charact.,* 2025, vol. 220, p. 114704. https://doi.org/10.1016/j.matchar.2024.114704

18. Zheng, Y., Zeng, W., Li, D., Xu, J., Ma, X., Liang, X., and Zhang, J., Orthorhombic precipitate variant selection in a Ti_2AlNb based alloy, *Mater. Des.,* 2018, vol. 158, pp. 46–61. https://doi.org/10.1016/j.matdes.2018.08.011

19. Zhu, F., Peng, H., Li, X., and Chen, J., Dissimilar diffusion bonding behavior of hydrogenated Ti_2AlNb-based and Ti–6Al–4V alloys., *Mater. Des.,* 2018, vol. 159, pp. 68–78. https://doi.org/10.1016/j.matdes.2018.08.034

20. Chu, Y., Li, J., Zhu, L., Tang, B., and Kou, H., Characterization of the interfacial-microstructure evolution and void shrinkage of Ti–22Al–25Nb orthorhombic alloy with different surface roughness during diffusion bonding, *Intermetallics,* 2017, vol. 90, pp. 119–127. https://doi.org/10.1016/j.intermet.2017.07.009

21. Hu, S.P., Hu, T.Y., Lei, Y.Z., Song, X.G., Liu, D., Cao, J., and Tang, D.Y., Microstructural evolution and mechanical properties of vacuum brazed Ti_2AlNb alloy and Ti60 alloy with Cu75 P t filler metal, *Vacuum,* 2018, vol. 152, pp. 340–346. https://doi.org/10.1016/j.vacuum.2018.03.054

22. Huang, K., Sun, H.-L., Huang, Z.-W., Liao, M.-Y., and Li, Y., Microstructure evolution and diffusion mechanism of Nb/TiAl alloy diffusion-bonded joints, *Rare Met.,* 2023, vol. 42, pp. 1686–1694. https://doi.org/10.1007/s12598-018-1125-8

23. Wang, Y., Cai, X.Q., Yang, Z.W., Wang, D.P., Liu, X.G., and Liu, Y.C., Diffusion bonding of Ti_2AlNb alloy using pure Ti foil as an interlayer, *J. Alloys Compd.,* 2018, vol. 756, pp. 163–174. https://doi.org/10.1016/j.jallcom.2018.04.324

24. Li, P., Ji, X., and Xue, K., Diffusion bonding of TA15 and Ti_2AlNb alloys: interfacial and microstructure and mechanical properties, *J. Mater. Eng. Perform.,* 2017, vol. 26, pp. 1839–1846. https://doi.org/10.1007/s11665-017-2555-4

25. Li, P., Wang, L., Yan, S., Meng, M., and Xue, K., Temperature effect on the diffusion welding process and mechanism of B2–O interface in the Ti_2AlNbbased alloy: A molecular dynamics simulation, *Vacuum,* 2020, vol. 173, p. 109118. https://doi.org/10.1016/j.vacuum.2019.109118

26. Li, X., Wang, G., Zhang, J., and Liu, Y., Electrically assisted superplastic forming/diffusion bonding of the Ti_2AlNb alloy sheet, *Int. J. Adv. Manuf. Technol.,* 2020, vol. 106, pp. 77–89. https://doi.org/10.1007/s00170-019-04458-8

27. Zhu, F., Chen, C., Li, X., and Chen, J., Role of thermal cycle in joining Ti–6Al–4V and Ti_2AlNb-based alloys through diffusion bonding and post heat treatment, *Mater. Charact.,* 2019, vol. 156, p. 109830. https://doi.org/10.1016/j.matchar.2019.109830

28. Huang, L., Lu, Y., Li, J., Li, C., Li, P., Zhao, D., Shi, S., Liu, X., Ma, X., and Dong, H., Investigation of interfacial microstructure and mechanical performance within TiAl to Ti_2AlNb alloy vacuum diffusion bonded joints, *Intermetallics,* 2024, vol. 174, p. 108436. https://doi.org/10.1016/j.intermet.2024.108436

29. Naumov, S.V., Panov, D.O., Chernichenko, R.S., Sokolovsky, V.S., Volokitina, E.I., Stepanov, N.D., Zherebtsov, S.V., Alekseev, E.B., Nochovnaya, N.A., and Salishchev, G.A., Structure and mechanical properties of welded joints from alloy based on VTI-4 orthorhombic titanium aluminide produced by pulse laser welding, *Izv. Non-Ferrous Metall.,* 2023, vol. 29, pp. 57–73. https://doi.org/10.17073/0021-3438-2023-2-57-73

30. Naumov, S., Panov, D., Sokolovsky, V., Chernichenko, R., Salishchev, G., Belinin, D., and Lukianov, V., Microstructure and mechanical properties of Ti_2AlNb based alloy weld joints as a function of gas tungsten arc welding parameters, *Obrab. Met. Work. Mater. Sci.,* 2025, vol. 27, pp. 43–56. https://doi.org/10.17212/1994-6309-2025-27.2-43-56